Thermoreversible Morphology Transition between Spherical and Cylindrical Microdomains of Block Copolymers†

Shinichi Sakurai,*,‡ Hiromitsu Kawada,§ and Takeji Hashimoto*

Department of Polymer Chemistry, Kyoto University, Sakyo-ku, Kyoto 606-01, Japan

Lewis J. Fetters

Corporate Research Laboratories, Exxon Research and Engineering Company, Annandale, New Jersey 08801

Received December 29, 1992; Revised Manuscript Received June 29, 1993®

ABSTRACT: Thermoreversible morphological transition (MT) of a poly(styrene-*block*-isoprene) diblock copolymer was studied by small-angle X-ray scattering (SAXS) and transmission electron microscopy (TEM). The cylindrical and spherical microdomains of polystyrene (PS) which are embedded in the polyisoprene matrix were thermoreversibly observed at 150 and 200 °C, respectively. As far as we know, this work may be the first to show that the cylindrical and spherical morphologies can reversibly change with temperature. Using experimentally determined interaction parameters χ, we compared SAXS and TEM results with the theory in the weak segregation limit presented by Leibler, which predicts the thermoreversible MT between spheres and cylinders. Consequently, $(\chi N)_t < (\chi N)_{200\,^\circ C} < (\chi N)_s < (\chi N)_1 < (\chi N)_{150\,^\circ C}$ was obtained, where $(\chi N)_t$, $(\chi N)_s$, and $(\chi N)_1$ denote the theoretical values of product χN at the microphase separation transition (MST), at the spinodal point of the MST, and at the MT between spheres and cylinders, respectively, and N is the degree of polymerization of the copolymer.

I. Introduction

Thermally induced morphological transition (MT) in a block copolymer has the potentiality to promote kinetic control of the morphology in various ways. This is a similar concept to the kinetic control of the morphology of polymer blends via spinodal decomposition.[1-3] Although the phase-separated structure in the block copolymers is considerably smaller than that in the polymer blends, physical properties of the block copolymers also strongly depend on their morphologies.[4-8] The use of a selective solvent for the solution casting of the block copolymer promotes morphology control[8-11] and the thermally induced morphology transition.[10,11] In this case a kinetically locked morphology can be formed in the as-cast specimen and the thermally induced transition from the kinetically locked morphology to an equilibrium morphology in melts has been definitely elucidated.[10,11]

Control of thermodynamically equilibrium morphology is another important aspect. The recent theories[12-16] in the weak segregation limit (WSL) predict that the morphology reversibly changes with segregation power and therefore with temperature. In Figure 1 the phase diagram by Leibler's WSL theory,[12] in which the so-called finite size effect[13-16] was not included, is schematically presented for molten A–B diblock copolymers having a UCST (upper critical solution temperature) type temperature dependence of the interaction parameter. The quantity f denotes the fraction of one of the block chains in the copolymer. According to this phase diagram based upon Landau type mean-field theory, with increasing temperature the equilibrium morphology changes from the lamellae to disordered state via cylinders and spheres, except for $f = 0.5$; this morphological change should be thermoreversible. As f approaches 0 or 1, the possible morphology is cylindrical or spherical. In the case of cylinders, the transition from cylinders to spheres should be necessarily detected with increasing temperature, prior to observation of the disordered state. However, the thermoreversible MT has not yet been experimentally confirmed. Difficulty in observing the thermoreversible MT may be because the narrow temperature range for the spherical phase causes the formation of the microdomains to be technically difficult.

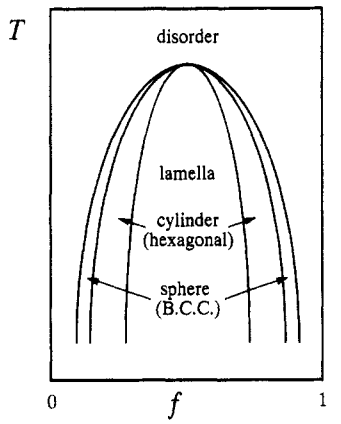

Figure 1. Schematic representation of the phase diagram by Leibler's weak segregation limit theory with UCST (upper critical solution temperature) type temperature dependence of the interaction parameter. According to this, it is possible to see equilibrium morphology changes from lamellar morphology to the disordered state via cylinders in the hexagonal lattice (hex) and spheres in the body-centered-cubic lattice (bcc) with increasing temperature, except $f = 0.5$.

In this study, a poly(styrene-*block*-isoprene) (SI) diblock copolymer was used in order to elucidate the thermoreversible MT by small-angle X-ray scattering (SAXS) and transmission electron microscopy (TEM). Since the

* To whom correspondence should be addressed.

† Presented in part before the 40th Annual Meeting of the Society of Polymer Science, Kyoto, Japan, May 1991. Sakurai, S.; Hashimoto, T.; Fetters, L. J. *Polym. Prepr., Jpn., Soc. Polym. Sci., Jpn.* **1991**, *40* (3), 770. Also published in part by: Sakurai, S.; Kawada, H.; Hashimoto, T.; Fetters, L. J. *Proc. Jpn. Acad., Ser. B* **1993**, *69*, 13.

‡ Present address: Department of Polymer Science and Engineering, Kyoto Institute of Technology, Matsugasaki, Sakyo-ku, Kyoto 606, Japan.

§ Present address: Kao Corporation, Sumida-ku, Tokyo 131, Japan.

® Abstract published in *Advance ACS Abstracts*, September 15, 1993.

0024-9297/93/2226-5796$04.00/0

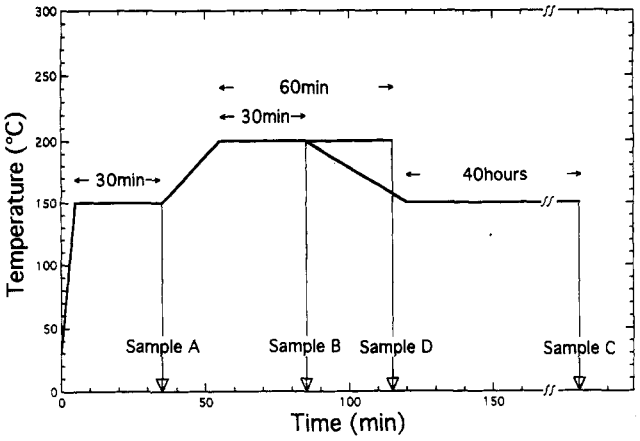

Figure 2. Temperature diagrams used for heat treatment for samples A–D.

copolymer was required to have sufficient mobility and the biased composition f, the SI with the small weight fraction of polystyrene (PS) (0.16) was utilized. Moreover, the specimens were sufficiently heat-treated at 150 and 200 °C so as to improve regularity in the ordering of the microdomains. The ultrathin sectioning was performed by cryoultramicrotomy at −85 °C so as to prevent the microdomain structure from deformation by the sectioning. The cylindrical and spherical microdomains of PS in the polyisoprene (PI) matrix were thermoreversibly observed at 150 and 200 °C, respectively. A short paper was reported on this thermoreversible MT as observed by TEM.[17] In the current paper we will describe full details of this thermoreversible MT.

II. Experimental Section

The SI specimen coded as SI-16/82 was anionically synthesized in cyclohexane/benzene (30 °C) with *sec*-butyllithium as the catalyst. The details of the synthesis are described elsewhere.[18] The number-average molecular weight, M_n, and the heterogeneity index, M_w/M_n, were determined to be 8.2×10^4 and 1.05 by membrane osmometry and size exclusion chromatography, respectively, where M_w designates the weight-average molecular weight. The weight fraction of PS, w_{PS}, was analyzed by ^{1}H NMR to be 0.16. The volume fraction of PS, f_{PS}, was calculated to be 0.15 using the densities 0.970 and 0.899 g/cm^3 for PS at 373 K ($>T_{g,PS}$) and for 1,4-PI at 298 K, respectively.[19] The microstructures in the PI blocks characterized by ^{1}H NMR were 93 and 7% for 1,4- and 3,4-linkages, respectively. The film specimens were obtained from a toluene solution of *ca.* 5 wt % polymer concentration by evaporating the solvent. Since the solubility parameter values[20] are 7.9–8.4, 8.6–9.7, and 8.9 (cal/cm^3)$^{1/2}$ for PI, PS, and toluene, respectively, toluene can be approximated as a neutral solvent for SI.

The as-cast specimen was subjected to thermal annealing at 150 and 200 °C under vacuum. The temperature diagrams used for the heat treatments are shown in Figure 2. First, the as-cast specimen was heated up to 150 °C and then held at this temperature for 30 min. Then the specimen designated as sample A was obtained by immediately quenching it in an ice/water mixture. For the other specimens, the temperature was further raised to 200 °C and kept there for 30 min. Then the specimen designated as sample B was obtained by immediately quenching the sample in the ice/water mixture. For sample C, temperature was cooled down again to 150 °C, kept there for 40 h, and then quenched in the ice/water mixture. Sample D has a thermal history similar to that of sample B. The difference between samples B and D lies in the holding times at 200 °C, i.e., 30 and 60 min for samples B and D, respectively. These specimens were subjected to SAXS and TEM experiments. It is noted here that the kinetically locked morphology in the as-cast specimen,[9-11] if any, may be erased by the first thermal annealing at 150 °C for 30 min.

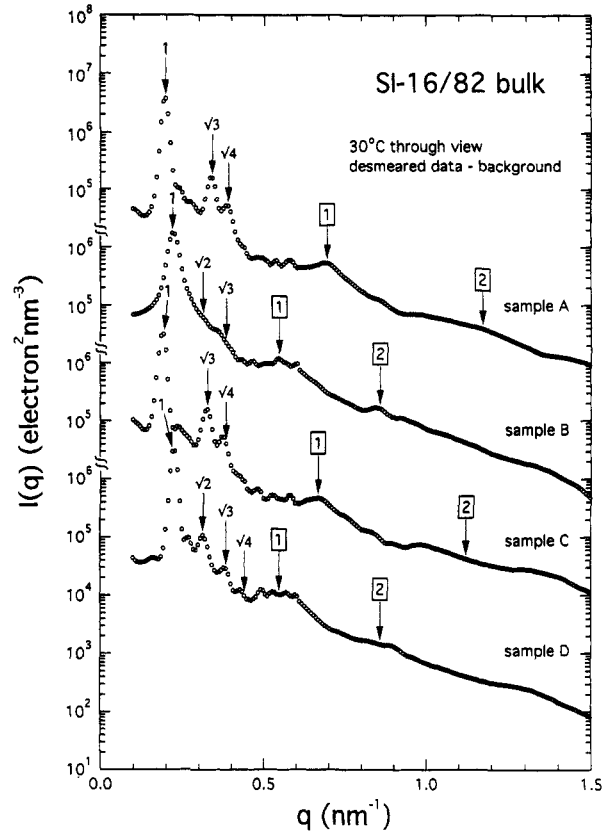

Figure 3. Semilogarithmic plots of the desmeared absolute scattered intensity $I(q)$ vs q for throughviews of the heat-treated SI-16/82 specimens, samples A–D.

SAXS measurements were performed at room temperature with an apparatus[21] consisting of a 12-kW rotating-anode X-ray generator, a graphite crystal for the incident beam monochromatization, a 1.5-m camera, and a one-dimensional position-sensitive proportional counter (PSPC). Cu Kα radiation with a wavelength, λ, of 0.154 nm was used. The incident beam with a line-shaped cross-section was irradiated, and the scattered X-rays were collected with the one-dimensional PSPC which was horizontally set. The film normal was parallel to the propagation direction of the incident beam, i.e., the throughview geometry. The measured scattered intensities were further corrected for absorption due to the specimen, air scattering, thickness of the specimen, and thermal diffuse scattering arising from density fluctuations. The absolute scattered intensity was obtained by the nickel-foil method.[22] The measured scattered intensity as a function of a scattering angle, which is called hereafter the SAXS profile, is subjected to desmearing by the method described elsewhere[23] to eliminate the collimation error.

TEM was conducted in order to confirm the morphology analyzed by SAXS. The ultrathin sectioning was performed by cryoultramicrotomy at −85 °C, below T_g of PI (T_g = −68 °C[19]), to attain the rigidity of the specimen, using a Reichert Ultracut E low-temperature sectioning system. A Hitachi H-600 transmission electron microscope operated at 100 kV was used for the TEM of ultrathin sections of the specimens stained with osmium tetraoxide (OsO_4).

III. Results

In Figure 3, the desmeared SAXS profiles are presented in a semilogarithmic plot of the absolute scattered intensity vs the magnitude of the scattering vector, q, which is given by

$$q = |\mathbf{q}| = (4\pi/\lambda) \sin(\theta/2) \quad (1)$$

with θ and λ being the scattering angle and the wavelength of X-rays, respectively. These profiles were obtained at room temperature. For samples A and C, the profiles are almost the same and the scattering maxima can be detected

Table I. Results of SAXS and Fraction of Particle Calculated Assuming the Respective Morphology

sample	temp (°C)	spacing d^a (nm)	morphology	interdomain distance[b] (nm)	R^c (nm)	ϕ^d
A	150	31.6	cylinders in hexagonal lattice	36.5	7.16	0.140
B, D	200	28.6	spheres in sc lattice	28.6	10.6	0.213
			spheres in bcc lattice	35.0	10.6	0.151
			spheres in fcc lattice	35.0	10.6	0.164
			cylinders in hexagonal lattice	33.0	9.12	0.277
C	150	32.7	cylinders in hexagonal lattice	37.8	7.47	0.142

[a] d is evaluated from the position of the first-order lattice scattering peak. $d = d_{100}$ for hexagonal, $d = d_{100}$ for simple cubic (sc), $d = d_{110}$ for body-centered-cubic (bcc), and $d = d_{111}$ for face-centered-cubic (fcc) symmetry. [b] The interdomain distance is given by $(4/3)^{1/2} d_{100}$ for hexagonal, d_{100} for sc, $(3/2)^{1/2} d_{110}$ for bcc and $(3/2)^{1/2} d_{111}$ for fcc symmetry. [c] R = radius for cylinder or sphere. [d] ϕ = volume fraction of cylinder or sphere.

at relative q values of 1, $\sqrt{3}$, and $\sqrt{4}$. These are the diffraction peaks from hexagonally packed cylinders. The values of Bragg's spacing d, which are evaluated from the positions of the first-order lattice scattering peak, were 31.6 and 32.7 nm, respectively, for samples A and C. On the other hand, the maxima at the relative q values of 1, $\sqrt{2}$, and $\sqrt{3}$ are detected with d = 28.6 nm for both samples B and D. These may be ascribed to the spheres arranged in a cubic lattice. Note here that $d = d_{100}$ for hexagonal, $d = d_{100}$ for simple cubic (sc), $d = d_{110}$ for body-centered-cubic (bcc), and $d = d_{111}$ for face-centered-cubic (fcc) symmetry, where d_{hkl} is the spacing for (hkl) planes. It should be noted here that the $\sqrt{2}$ and $\sqrt{3}$ peaks are better defined for sample D than for sample B, implying that the spherical microdomains can have a higher order with the longer annealing time at 200 °C. This will be confirmed by TEM later on.

In Figure 3, at least one scattering maximum due to the isolated particle can be clearly seen for every sample at the position indicated by an arrow labeled with a number 1 in the square symbol. In some cases even the second-order maximum of the particle scattering can be discerned at the position indicated by an arrow labeled with a number 2 in the square symbol. From its q value the average value of the radii of the cylinders or spheres, R, is estimated using the following equations for the scattering maxima from the isolated particle:[11,24]

$$q_{p,i}R = 4.98, 8.364, 11.46, \ldots \quad \text{for cylinder; } i = 1, 2, 3, \ldots \quad (2)$$

$$q_{p,i}R = 5.765, 9.10, 12.3, \ldots \quad \text{for sphere; } i = 1, 2, 3, \ldots \quad (3)$$

where $q_{p,i}$ denotes the q value of the ith-order particle scattering peak. The values of d calculated from the position of the first-order diffraction maximum and R from $q_{p,1}$ are summarized in Table I. Assuming perfect hexagonal packing of the cylinders and noting that $d = d_{100}$, the volume fraction of the cylindrical microdomains, ϕ, is given as:[11]

$$\phi = \frac{\sqrt{3}}{2}\pi\left(\frac{R}{d_{100}}\right)^2 \quad (4)$$

For the spherical microdomains the following three types of lattices can be considered, i.e., sc, bcc, and fcc symmetries, for which $d = d_{100}$, d_{110}, and d_{111}, respectively. Assuming perfect packing, the volume fraction of the spherical microdomains, ϕ, is derived as:

$$\phi = \frac{4}{3}\pi\left(\frac{R}{d_{100}}\right)^3 \quad \text{for sc} \quad (5)$$

$$\phi = \frac{\sqrt{8}}{3}\pi\left(\frac{R}{d_{110}}\right)^3 \quad \text{for bcc} \quad (6)$$

$$\phi = \frac{16}{27}(3)^{1/2}\pi\left(\frac{R}{d_{111}}\right)^3 \quad \text{for fcc} \quad (7)$$

The values ϕ estimated by assuming a respective morphology are summarized in Table I. It is needless to say that the values ϕ calculated assuming the hexagonally packed cylinders for samples A and C are consistent with the f_{PS} value (0.15). The bcc lattice gives the best result among the four types of morphology for samples B and D. Thus SAXS definitely revealed the thermoreversible MT between cylinders at 150 °C and spheres at 200 °C.

In order to visually confirm the thermoreversible MT revealed by SAXS, we conducted TEM observations. Figures 4–7 show TEM photographs for samples A–D where the dark domains correspond to the PI microdomains stained with OsO_4 and the bright ones to the unstained PS microdomains. Generally speaking, the cylindrical microdomains of PS in the PI matrix phase were observed for samples A and C in Figures 4 and 6, respectively, while PS spheres in the PI matrix were seen for samples B and D in Figures 5 and 7, respectively. These results are well consistent with the SAXS results.

Let us examine the TEM micrographs in more detail. The hexagonally packed PS cylinders are observed for sample A, as shown in Figure 4. In some regions, the orientation direction of the cylinder axes is approximately parallel to the thin section. For sample B, PS spheres in the PI matrix are clearly seen in Figure 5. Figure 6 clearly shows hexagonally packed PS cylinders for sample C which was annealed at 150 °C for 40 h (see Figure 2). Owing to the long annealing time, the degree of ordering of the cylinders seems to be better than that of sample A. The micrograph shows a grain structure, within which the cylinder axes are oriented nearly parallel to each other. The grain boundary is formed at the place where the grains having different orientations of the cylinder axes meet each other. The cylinders in sample C seem to be packed in larger grains than those in sample A. Highly ordered PS spheres with large grains are also successfully obtained for sample D as shown in Figure 7. Upper (about $^2/_3$) and lower parts of the micrograph in part a are the bcc lattices having different orientations. Thus the grain boundary appears to run horizontally in this micrograph. A similar grain structure is also seen in part b. Comparison between Figures 5 and 7 may indicate that sample D has a higher order than sample B. The higher degree of ordering in sample D was manifested itself in the SAXS profiles, and this is due to a slightly longer annealing time for sample D as compared to sample B. It is interesting to note that the projection of the ordered PS spheres onto (*100*) and (*111*) planes of the bcc lattice can be unambiguously observed in parts a and b of Figure 7, respectively.

IV. Discussion

The thermoreversible MT between cylinders and spheres was complementarily observed by SAXS and TEM. As far as we know, this work may be the first to show that the cylindrical and spherical morphologies can be reversibly changed by changing temperature. There are some theoretical works concerning a phase diagram of the microphase structure of block copolymers in the strong segregation limit (SSL) and the WSL. In general, the

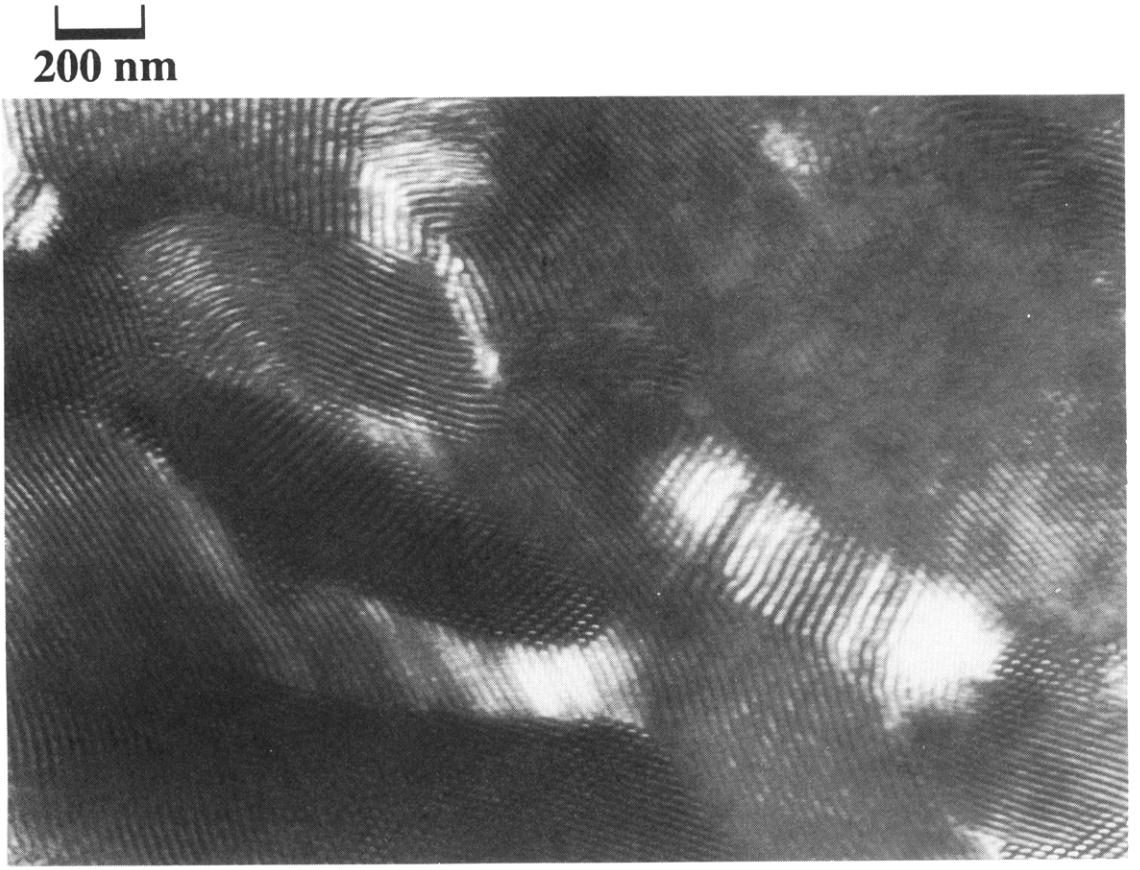

Figure 4. Transmission electron micrograph of sample A.

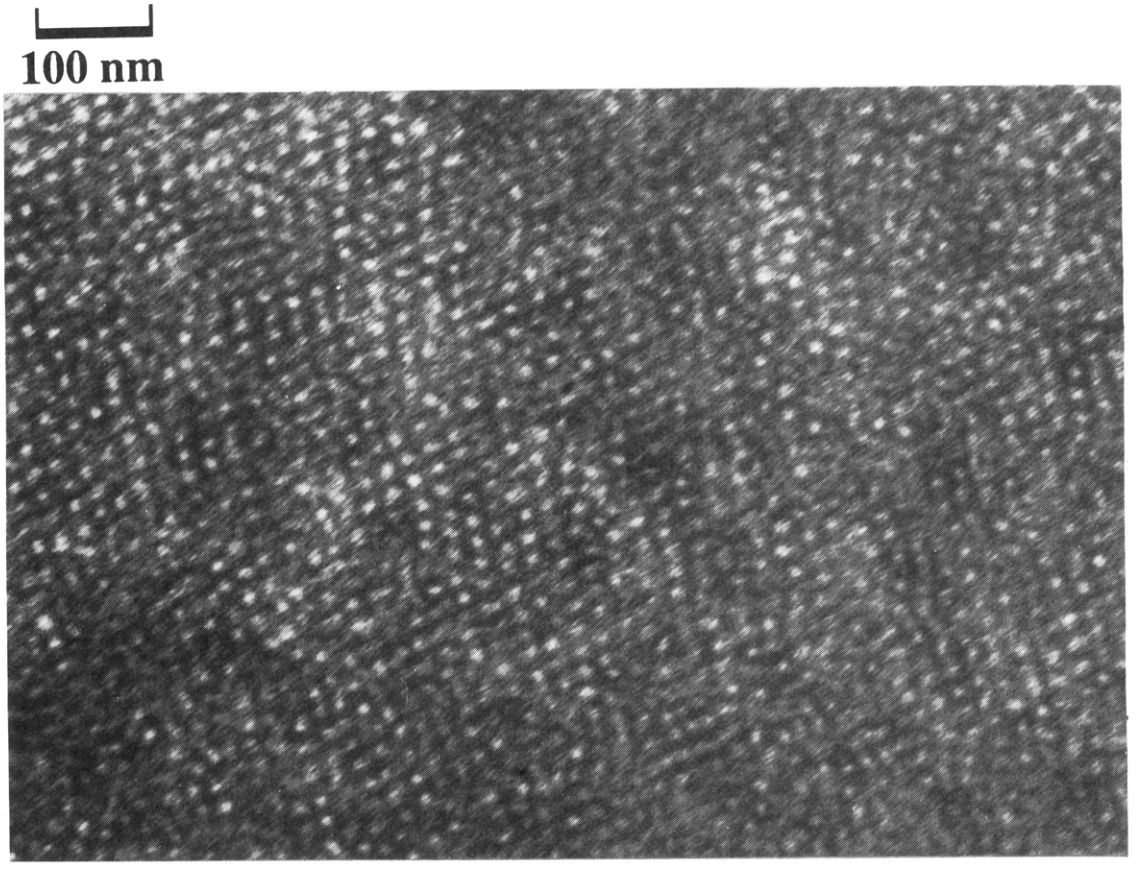

Figure 5. Transmission electron micrograph of sample B.

SSL theories[25–27] do not predict the morphological change with temperature for any given composition f. On the other hand, the WSL theories[12–16] predict the morphological change with temperature at a fixed f, if the value of f is not one of the exceptional values. Developments of the WSL theory have been done by Leibler.[12] He has

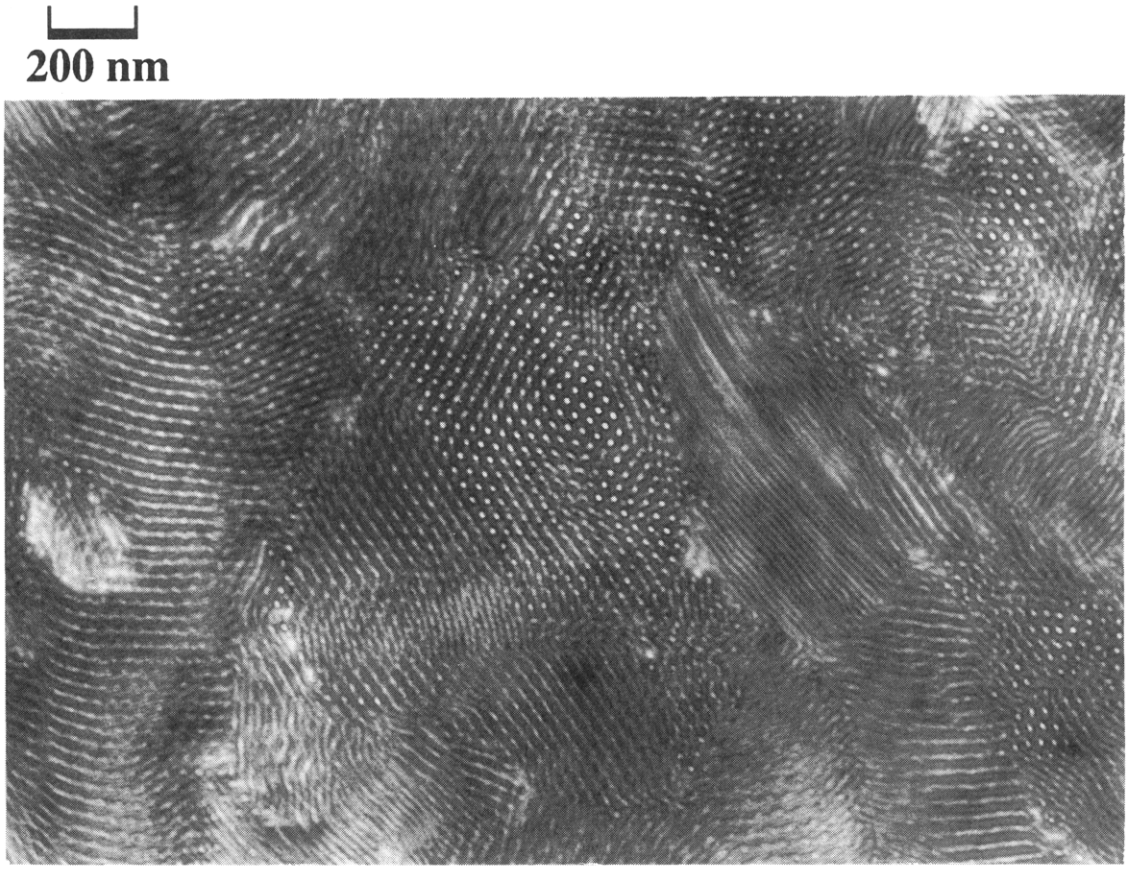

Figure 6. Transmission electron micrograph of sample C.

constructed a Landau expansion of the free energy in terms of a compositional order parameter. Random phase approximation (RPA) has been employed to compute the coefficients of the Landau expansion. He discussed the most favorable morphology of the microphase structure that appeared upon the microphase-separation transition (MST) by assuming that the structure may have spatial periodicity identical to $2\pi/q^*$ of the q Fourier mode, q^*, at which the correlation function diverges upon the MST. Fredrickson and Helfand have applied Brazovskii's Hartree analysis[28] to Leibler's mean-field theory. Namely, a Hartree approximation was used to demonstrate a fluctuation-induced first-order phase transition, instead of a second-order transition predicted by Leibler's theory, for the finite values of degree of polymerization N (so-called finite size effect). However, the Hartree approximation was found to be inapplicable to $N < 10^4$, as pointed out in their paper. Another important correction mentioned by Leibler is that for the polydispersity effect, which has recently been considered by Burger et al.[16] by averaging the response functions of the Gaussian copolymer chains assuming the Schultz–Zimm molecular weight distribution. Although they have also taken into account the finite size effect based on Brazovskii's Hartree analysis, their result of a computation cannot be used for comparison with our experimental results because N of the SI-16/82 used in our experiment is less than 10^4 ($N = 1139$). As a matter of fact, Figure 12 in their corrected issue[16] clearly shows that there are no bcc (sphere) regions for $N = 10^3$ and $(N_w/N_n)_K \leq 1.1$ (K = A or B). Here, N_w and N_n denote the weight- and number-average degrees of polymerization, respectively.

Let us compare the experimental results with Leibler's theory because this is the only one that predicts the thermoreversible MT between the spheres (bcc) and the cylinders (hex) for our copolymer. For $f = 0.15$, the computation according to his theory gave $(\chi N)_t = 36.41$, $(\chi N)_s = 38.04$, and $(\chi N)_1 = 38.94$ where $(\chi N)_t$, $(\chi N)_s$, and $(\chi N)_1$ denote the values of product χN at the MST, at the spinodal point of the MST, and at the MT between bcc and hex, respectively. For quantitative comparison, we employ here the temperature dependence of the interaction parameter χ_{SI} values for SI-16/82.

$$\chi_{SI} = -0.0258 + 27.9/T \tag{8}$$

This relationship was obtained experimentally from analyses of scattering profiles in the disordered state according to the method reported previously,[29,30] which includes corrections for polydispersity, composition distribution, and asymmetric effects on the scattering profile. The SAXS measurements were done with (SI-16/82)/DOP solutions at $\phi_{poly} = 0.72$ and 0.82. Here, DOP and ϕ_{poly} stand for dioctyl phthalate and the volume fraction of polymer in the solution, respectively. In order to evaluate bulk χ_{SI} values from the effective values, χ_{eff}, which were obtained for the solutions, the dilution approximation as expressed by $\chi_{SI} = \chi_{eff}/\phi_{poly}$ was used. Fredrickson and Leibler showed that even in the WSL there is a tendency for a neutral, good solvent to accumulate at the interface of the microdomains and concluded that the dilution approximation is irrelevant.[14] Moreover, in a rigorous sense, technically this dilution approximation is only valid when the solution of the block copolymer meets the optical Θ condition.[31] Note that the relationship given by eq 8 is only an approximation obtained by assuming the dilution approximation, although (SI-16/82)/DOP solutions do not meet rigorously the optical Θ condition. Since eq 8 is the only result available to χ for this copolymer at present, we attempt to use this result for the following discussion. Equation 8 gives $(\chi N)_{150\,°C} = 45.71$ and $(\chi N)_{200\,°C} = 37.78$ which leads to $(\chi N)_t < (\chi N)_{200\,°C} < (\chi N)_s < (\chi N)_1 <$

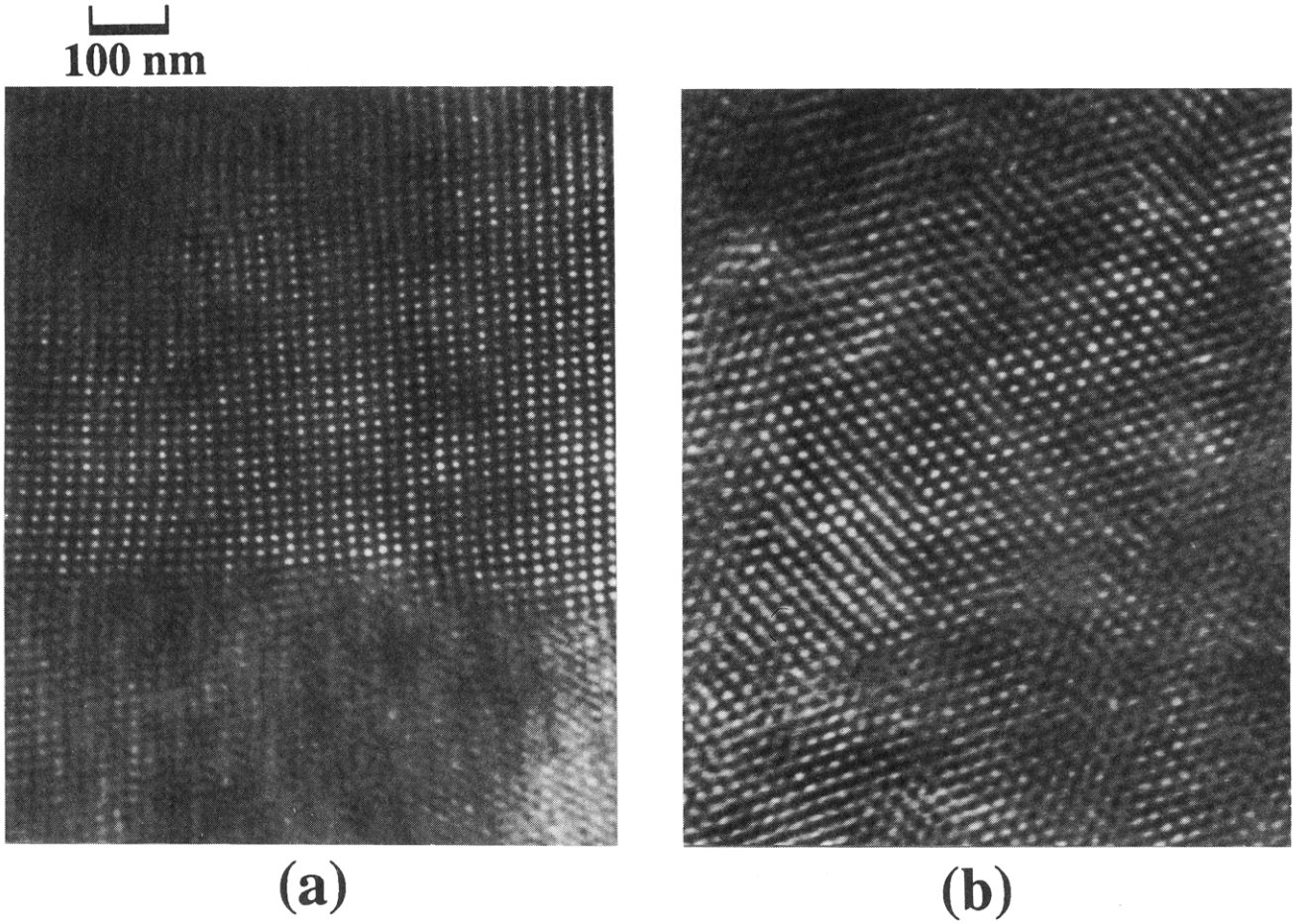

Figure 7. Transmission electron micrographs of sample D. The projections of the ordered PS spheres onto (*100*) and (*111*) planes of the bcc lattice can be seen in parts a and b, respectively.

$(\chi N)_{150\ °C}$.[32] This indicates that the most favorable morphologies are spheres at 200 °C and cylinders at 150 °C according to Leibler's theory. These are in good accord with the experimental results.

Although we showed above that Leibler's WSL theory works well to describe the thermoreversible MT of the current study, there is crucial disagreement between the WSL theory and the experimental findings. The WSL theory assumes that the spatial periodicity does not change with χN even if the system goes far away from the MST. In other words, the WSL theory does not deal with copolymer chains stretched in the microdomain space. However, an increase of the spatial periodicity with a decrease of temperature (i.e., with an increase of χ) was observed in this study. Furthermore, it has generally been recognized that the block chain in the microdomain is more or less stretched in the direction normal to the interface owing to the segregation between the different types of block chains.[33-36] Therefore, a new theory that describes the crossover from the WSL to the SSL by including effects of a chain stretching is definitely required for the explanation of the thermoreversible MT relevant to the current study. Since this kind of theory is not available at present, let us present below a qualitative picture of possible models about the thermoreversible MT.

Figure 8 schematically presents chain conformations in two morphologies of cylinders and spheres for a molten A–B diblock copolymer with a large asymmetry in block chain lengths, i.e., $N_A \gg N_B$, where N_A and N_B denote the degrees of polymerization for A and B block chains, respectively. The asymmetry in N_A and N_B involves an asymmetry in the radii of gyration $R_{gA,\parallel}$ and $R_{gB,\parallel}$ as well

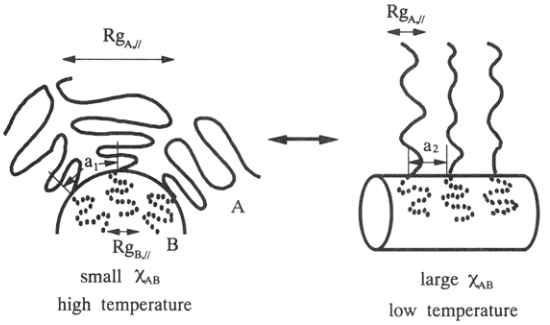

Figure 8. Schematic representation showing chain conformations in two morphologies of (a) spheres and (b) cylinders for a molten A–B diblock copolymer with a large asymmetry in block chain lengths, i.e., $N_A \gg N_B$, where N_A and N_B denote the degrees of polymerization for A and B block chains, respectively.

as an asymmetry in the overall radii of gyration R_{gA} and R_{gB} where $R_{gK,\parallel}$ denotes the radius of gyration of K block chains (K = A or B) parallel to the interface between A and B microdomains. Due to the requirement that K block chains must be uniformly placed in the K microdomains while satisfying the demand of incompressibility ($\rho_A = \rho_{A,0}$ and $\rho_B = \rho_{B,0}$), the conformations of K block chains may be like those as shown in Figure 8. Here ρ_K and $\rho_{K,0}$ are the segmental densities of the K component in a microdomain space and a free space, respectively. In the model shown in part a as in the case of the spherical morphology, the requirement of the spatial placement of the asymmetric block chains is realized by introducing a curvature in the interface. On the other hand, in the model shown in part b for the cylindrical morphology, the requirement is realized by further stretching the A block

chains normal to the interface and hence by further reducing the average asymmetry in $R_{gA,\|}$ and $R_{gB,\|}$. This model in part b for cylindrical microdomains invokes a reduction of mean curvature of the interface compared to that of the spherical microdomains shown in part a.

The extra stretching of the A block chains, however, invokes shrinking of the average area occupied by the copolymer chain at the interface from a_1^2 to a_2^2 in order to satisfy the demand of incompressibility. The model in part a has a greater conformational entropy and a larger interfacial area per block chain (comparing a_1^2 to a_2^2) than the model in part b. Thus the spheres are less favorable than the cylinders when the free energy associated with the energetic interaction between A and B plays a dominant role on the microdomain formation. On the other hand, if the free energy associated with the conformational entropy is dominant in the microdomain formation, the spheres are more favorable than the cylinders.

For the UCST type A–B interaction (in which interaction decreases with increasing temperature) as in our SI diblock copolymer, as temperature is raised, the energetic interaction contribution is outweighed by the conformational entropy contribution and hence the spheres shown in part a become more favorable than the cylinders shown in part b. However, as temperature is lowered, the energetic contribution outweighs the conformational entropy contribution, and hence the cylinders become more favorable than the spheres.

V. Concluding Remarks

The thermoreversible morphology transition between cylinders and spheres was complementarily observed by SAXS and TEM. As far as we know, this work may be the first to show that the cylindrical and spherical morphologies can be reversibly changed by changing temperature. Recently, Almdal et al.[37] have reported order–order transitions with temperature in a poly(ethylenepropylene-*block*-ethylethylene) (PEP–PEE) diblock copolymer studied using small-angle neutron scattering (SANS) and rheological measurements. The multiple ordered phases that they have determined by SANS using shear-oriented samples are lamellar and two unidentified new morphologies other than either cylinders or spheres. Note that we applied no such special external field as shear to identify the morphology in the current study. Moreover, we have explored a stronger segregation regime using the SI diblock copolymer, as compared to using the PEP–PEE. Thus the MT observed by us seems to be quite different from that observed by Almdal et al.

Although Leibler's WSL theory agreed with the experimental results in this particular case of the thermoreversible MT of the current study, there is a crucial fault in the WSL theory such that it does not include the chain stretching in the microdomains. Therefore, the theory which describes the crossover from the WSL to the SSL is definitely required for the explanation of the thermoreversible MT relevant to the current study. More experimental studies are also necessary to make a quantitative comparison between experiments and theories.

Acknowledgment. The authors are grateful to K. Iwane for his help on heat treatments of specimens.

References and Notes

(1) Nose, T. *Phase Transitions* **1987**, *8*, 245.
(2) Hashimoto, T. *Phase Transitions* **1988**, *12*, 47.
(3) Tran-Cong, Q.; Nagaki, T.; Yano, O.; Soen, T. *Macromolecules* **1991**, *24*, 1505.
(4) Kawai, H.; Hashimoto, T.; Miyoshi, K.; Uno, H.; Fujimura, M. *J. Macromol. Sci., Phys.* **1980**, *B17* (3), 427.
(5) Molau, G. E. In *Block Polymers*; Aggarwal, S. L., Ed.; Plenum Press: New York, 1970.
(6) Hashimoto, T.; Shibayama, M.; Fujimura, M.; Kawai, H. In *Block Copolymers: Science and Technology*; Meier, D. J., Ed.; MMI Press and Harwood Academic Publisher: New York, 1983.
(7) Hashimoto, T. In *Thermoplastic Elastomers*; Legge, N. R., Holden, G., Schroeder, H. E., Eds.; Hanser: Munich, 1987.
(8) Sakurai, S.; Sakamoto, J.; Shibayama, M.; Nomura, S. *Macromolecules* **1993**, *26*, 3351.
(9) Cohen, R. E.; Bates, F. S. *J. Polym. Sci., Polym. Phys. Ed.* **1980**, *18*, 2143.
(10) Sakurai, S.; Hasegawa, H.; Hashimoto, T. *Polym. Prepr., Jpn., Soc. Polym. Sci., Jpn.* **1990**, *39* (3), 387. Sakurai, S.; Kawada, H.; Shiwaku, T.; Hashimoto, T., in preparation.
(11) Sakurai, S.; Momii, T.; Taie, K.; Shibayama, M.; Nomura, S.; Hashimoto, T. *Macromolecules* **1993**, *26*, 485.
(12) Leibler, L. *Macromolecules* **1980**, *13*, 1602.
(13) Fredrickson, G. H.; Helfand, E. *J. Chem. Phys.* **1987**, *87*, 697.
(14) Fredrickson, G. H.; Leibler, L. *Macromolecules* **1989**, *22*, 1238.
(15) Olvera de la Cruz, M. *J. Chem. Phys.* **1989**, *90*, 1995.
(16) Burger, C.; Ruland, W.; Semenov, A. N. *Macromolecules* **1990**, *23*, 3339. A correction appeared in *Macromolecules* **1991**, *24*, 816.
(17) Sakurai, S.; Kawada, H.; Hashimoto, T.; Fetters, L. J. *Proc. Jpn. Acad., Ser. B* **1993**, *69*, 13.
(18) Morton, M.; Fetters, L. J. *Rubber Chem. Technol.* **1975**, *48*, 359.
(19) Fetters, L. J., unpublished results.
(20) Grulke, E. A. In *Polymer Handbook*, 3rd ed.; Brandrup, J., Immergut, E. H., Eds.; Wiley: New York, 1989.
(21) Hashimoto, T.; Suehiro, S.; Shibayama, M.; Saijo, K.; Kawai, H. *Polym. J. (Tokyo)* **1981**, *13*, 501.
(22) Hendricks, R. W. *J. Appl. Crystallogr.* **1972**, *5*, 315.
(23) Fujimura, M.; Hashimoto, T.; Kawai, H. *Mem. Fac. Eng., Kyoto Univ.* **1981**, *43* (2), 224.
(24) Tanaka, H.; Hasegawa, H.; Hashimoto, T. *Macromolecules* **1991**, *24*, 240.
(25) Helfand, E.; Wasserman, Z. R. In *Developments in Block Copolymers-1*; Goodman, I., Ed.; Applied Science Publishers: New York, 1982.
(26) Semenov, A. N. *Sov. Phys. JETP* **1985**, *61*, 733.
(27) Ohta, T.; Kawasaki, K. *Macromolecules* **1986**, *19*, 2621. Kawasaki, K.; Ohta, T.; Kohrogui, M. *Macromolecules* **1988**, *21*, 2972.
(28) Brazovskii, S. A. *Sov. Phys. JETP* **1975**, *41*, 85.
(29) Sakurai, S.; Mori, K.; Okawara, A.; Kimishima, K.; Hashimoto, T. *Macromolecules* **1992**, *25*, 2679.
(30) Tanaka, H.; Sakurai, S.; Hashimoto, T.; Whitmore, M. D. *Polymer* **1992**, *33*, 1006.
(31) Hashimoto, T.; Mori, K. *Macromolecules* **1990**, *23*, 5347.
(32) The correction for asymmetry in segmental volumes[29,30] should be considered in the degree of polymerization, N. For this correction, N is replaced by r_C where $r_C = (N_A v_A + N_B v_B)/v_0$ with v_K [$=M_{u,K}/\rho_K$] and v_0 [$=(v_A v_B)^{1/2}$] being the segmental volume of the K component (K = A or B) and the reference cell volume, respectively. $M_{u,K}$ and ρ_K stand for the molecular weight of a repeating unit and the density of the K component, respectively. As a result, $r_c = 1002$ is obtained, and this leads to $(\chi r_c)_{200\,°C} = 33.23 < (\chi N)_t < (\chi N)_s < (\chi N)_1 < (\chi r_c)_{150\,°C} = 40.21$. It is consistent with the experimental result at 150 °C (cylinders) but not consistent with that at 200 °C (spheres). Although more precise data on χ_{SI} than eq 8 are required to check this discrepancy, further quantitative discussion is beyond the scope of this paper. It can be stated that Leibler's theory qualitatively agrees with the experiments with respect to cylinders at lower temperature and spheres at higher temperature.
(33) Hadziioannou, G.; Picot, C.; Skoulios, A.; Ionescu, M.-L.; Mathis, A.; Duplessix, R.; Gallot, Y.; Lingelser, J.-P. *Macromolecules* **1982**, *15*, 263.
(34) Hasegawa, H.; Hashimoto, T.; Kawai, H.; Lodge, T. P.; Amis, E. J.; Glinka, C. J.; Han, C. C. *Macromolecules* **1985**, *18*, 67.
(35) Hasegawa, H.; Tanaka, H.; Hashimoto, T.; Han, C. C. *Macromolecules* **1987**, *20*, 2120; *J. Appl. Crystallogr.* **1991**, *24*, 672.
(36) Matsushita, Y.; Mori, K.; Mogi, Y.; Saguchi, R.; Noda, I.; Nagasawa, M.; Chang, T.; Glinka, C. J.; Han, C. C. *Macromolecules* **1990**, *23*, 4317.
(37) Almdal, K.; Koppi, K. A.; Bates, F. S.; Mortensen, K. *Macromolecules* **1992**, *25*, 1743.